JEAS

Journal of Engineering and Applied Sciences 3 (2007) 61 - 66

JOURNAL OF ENGINEERING AND

Application of GIS technique to the interpretation of the aeromagnetic map and landsat imagery of Buji Younger Granite Complex, northern Nigeria

F.X.O. Ugodulunwa, *H.M. Yakubu

*Department of Geology and Mining, University of Jos, Jos, Nigeria *Osara Campus, Kogi State Polytechnic, Lokoja, Kogi State, Nigeria*

Abstract

Analysis of digitized total intensity magnetic field map of the Buji Younger Granite Complex and environs revealed three major trends of magnetic lineaments, in the northeast-southwest, northwest-southeast, and north-south directions. Application of gradient filters in the X(east) and Y(north) directions showed these lineaments clearly. The lineaments may represent structural trends in the underlying rocks. Some digitized lineaments on the landsat imagery of the area coincide with sections of the drainage system, which suggests that the drainage system may be structurally controlled. The lineaments from the landsat imagery and some fractures observed during fieldwork show four major directions namely, north-south, east-west, northeast-southwest and northwest-southeast. The north-south trend may be due to an imprint of the Pan African Orogeny, while the northeast-southwest and northwest-southeast may be conjugate fractures superimposed on the north-south structures. The length-azimuth graphs show that the longest lineaments trend N57^o W for landsat lineaments, and N20^o E for fractures observed in the field. Histograms of these data show a tri-modal distribution for the landsat lineaments and a northward clustering for the fractures observed in the field. Rocks of the Buji Complex have lower magnetic intensity than rocks of the surrounding Basement Complex.

1. Introduction

The Buji Complex is one of the Nigerian Younger Granite Ring Complexes. It is located about 15km north of Jos city and is bound by latitudes 10° 01'N and 10° 07'N, and longitudes 8° 49'E and 8° 36'E (Fig. 1). It is part of 1:50000 sheet 147, Lere South East. The Buji Complex is of interest partly because of its accessibility and comparatively small size when compared to many of the Nigerian Younger Granite Ring Complexes. Its structural characteristics, lithological relationships and economic potential can therefore be studied with relative ease.

1.1. Geology and water resources

The Buji Complex and the other Nigerian Younger Granite Ring Complexes were first described by Falconer (1911) after a reconnaissance survey. He distinguished between the Younger Granites and the Older Granites on the basis of their field relationships. The Younger Granites had cross-cutting relationships with the country rocks and chilled margins. They are also the source rocks for the tin mineralization of Jos Plateau. Macleod et. al (1971) and Jacobson et. al. (1958) carried out detailed geological survey of the Buji Complex. The area is underlain by migmatites and gneisses of the Basement Complex, Older Granites, volcanic rocks and hypabyssal rocks (Fig.2). The volcanic rocks include Early and Late Rhyolites, while the hypabyssal rocks include quartz-feldspar porphyry and quartz hedenbergite porphyry. Migmatites surround the Buji Complex to the east while gneisses, some of which are pegmatitic, occur to the west. Some of these rocks are also found uplifted on top of the Buji Complex. Buchanan et. al. (1971) also observed that the Buji Complex consists of two superimposed Younger Granite Complexes namely, the eastern complex and the western complex. The eastern complex was emplaced earlier and is composed entirely of volcanic rocks and high level intrusions. Granitic rocks predominate in the western complex. The area is well drained by many streams and their tributaries. Surface water

is supplemented by underground water stored in weathered bedrock and fractured crystalline rock aquifers. Fig. 3 shows the outline of the Buji Complex and the drainage system of the area.

2. Materials and methods

The datasets used in this work include Landsat imagery, aeromagnetic maps, topographic maps and data obtained during fieldwork. The satellite imagery was in digital format while the others were in analog format. The analog data were digitized and then processed along with the Landsat imagery to reveal aspects of the geology of the area.

2.1. Aeromagnetic data

The total intensity aeromagnetic map of 1:100,000 sheet 147 Lere was digitized. A base level datum of 25000nT was then applied to the data before contouring at 10nT interval (Fig 4). Next the Digital Elevation Model (DEM), and the gradient filtered maps in the X(east) direction (Dfdx), and Y(north) direction (Dfdy) were computed (Figs.5, 6 and 7). The DEM presents the spatial distribution of the magnetic intensity above some arbitrary datum in a landscape (Meer, 1997).

2.2. Topographic and landsat imagery data

Fig. 3 resulted from digitizing the topographic map of 1:50,000 sheet 147 Lere South-east. The landsat imagery of the study area taken in November 2000 is shown in Fig. 8. This imagery was processed in two stages to enhance the geological information it contains. One of the programs of the Integrated Land and Water Information System (ILWIS) academic 3.1 was first used to aggregate the imagery scene into rock classes based on their natural spectral values. This is referred to as unsupervised classification. Next, linear features on the imagery were digitized to produce lineament map of the area (Fig.9). Seventy-eight lineaments were digitized from the landsat Imagery.

2.3. Field fracture data

During fieldwork in the area, the lengths and orientations of 116 fractures were measured. Histograms and rose plots were drawn for the lineaments from the landsat imagery and the field fractures (Figs. 10, 11, 12 and 13). The histogram shows the number of lineaments (frequency) for each range of orientations while the rose plots are essentially radial histograms since all the lineaments were given equal weights.

3. Interpretation

3.1. Interpretation of aeromagnetic maps and landsat imagery

The Geographic Information System (GIS) makes it possible to compare information from different sources about a particular point of interest. Some attributes observed on various maps and datasets can then be interpreted with greater confidence. Such attributes may be related to particular geological structures or other events in the study area.

The magnetic anomalies on the aeromagnetic map can be grouped into three zones (Fig. 4). The anomalies located north of latitude 10° 5'N have strong east-west trend, while anomalies in the central and south-western areas have strong northeast-southwest trend. Anomalies in the east have north-south trend. The eastern contact of the Buji Complex with the Basement Complex trends northsouth. These trends show clearly on the Digital Elevation Model (DEM) map and the gradient filtered (Dfdx, Dfdy) maps (Figs 5, 6, 7). The intrusive rhyolites, tuffs and agglomerate that underlie the northern part of the Buji Complex have an east-west trend. They probably cause the high magnetic intensity labeled 'b' in Figure 4(a). The migmatites in the southeastern part of the study area also have high magnetic intensity (labeled 'h' in Figure 4(a)). The Buji biotite granite (labeled 'd' & 'e' in Figure 4(b)), also have higher magnetic intensity than the granite gneiss of the Basement Complex which they intrude. The magnetic closures and steep horizontal gradients observed on the aeromagnetic map are also related to the underlying geology. The axes of the closures define the trends stated above while the steep gradients mark the boundaries between different rock types.

Visual inspection of the landsat imagery shows the distinct outline of the Buji Complex surrounded by the low relief of the Basement Complex (Fig. 8). Clustering and unsupervised classification of the imagery reveal three broad classes of rocks namely, rocks of the Basement Complex, rocks of the Buji Complex and weathered rocks. The clustering also shows that the rocks of the Basement Complex are more deeply weathered than rocks of the Younger Granites of the Buji Complex.

3.2. Interpretation of lineaments from aeromagnetic and landsat data

Aeromagnetic surveys are very useful in mapping structural trends. Lineaments on the aeromagnetic maps often correspond to the strike lines of elongated geological features like dykes, fractures, faults and lithological boundaries. Alignment of one or more prominent features on a landsat imagery over a distance also appears as a lineament. It may be a topographic feature or an expression of underlying geological structure such as fracture, fault, dyke or lithological boundary.

Trend lines labeled AB, CD and EF on the Digital Elevation Model (DEM) map are magnetic lineaments (Fig. 5). They trend in the northeast-southwest, east-west and northeast-southwest directions respectively. When the lineament map was superimposed (draped) on the drainage

map of the study area there was remarkable correlation of the two maps (Fig. 9). Some of the areas where correlation was observed have been labeled a, b, c,…….k . River Gurum and River Delimi and major tributaries of River Gurugushele flow along some of the lineaments. One may conclude that part of the drainage system of the Buji Complex area is structurally controlled.

The histogram and rose plot of the fractures observed in the field showed tri-modal distribution along the NE-SW, NW-SE and N-S directions with a northward clustering from N20^o W to N60^o E (Figs. 12 and 13).The histogram and rose plot of the lineaments from the landsat imagery showed tri-modal distributions along N-S, NE-SW and NW-SE directions with minor E-W direction (Figs. 10 and 11).

4. Discussion

Detailed digital analysis of the aeromagnetic map and landsat imagery of the Buji Complex area in a GIS environment showed three major lineament directions namely,
NE-SW, NW-SE and N-S as shown on the histograms and rose plots. The E-W direction was minor although it showed clearly on the aeromagnetic, DEM and gradient filtered maps. The consistency of these lineaments points to their geological significance. They represent lithological contacts, and underlying fractures and faults.

The NW-SE lineaments were not obvious on the aeromagnetic map but they were observed during fieldwork and on the landsat imagery. This difference may be explained by the fact that the magnetic anomalies reflect the history and distribution of magnetic minerals in the rocks while the landsat imagery records many different attributes of each rock. Fractures and faults result from the action of stress forces on the rock as a whole. The N-S lineaments may be linked to the Pan African orogeny while the NE-SW and NW-SE lineaments may due to younger conjugate fractures in the Basement Complex.

North-south and northwest-southeast profiles across the aeromagnetic map showed that rocks of the Buji Younger Granite Complex are more magnetic than thegneisses of the Basement Complex but less magnetic than the migmatites. Rocks of the Basement Complex are more deeply weathered than the rocks of the Buji Younger Granite Complex. The Younger Granite Complex therefore occurs as a prominent topographic feature. Part of the drainage system in the area is structurally controlled. This is probably because of the deep fractures that traverse the area.

5. Conclusion

The interpretation of digitally processed aeromagnetic data and Landsat imagery of the Buji Younger Granite Complex was greatly enhanced by the application of Global Information System (GIS). It enabled direct correlation of features observed on various datasets with the geology. It also enabled broad classification of the underlying rocks. The area is intensely fractured, and the rocks of the Buji Younger Granite Complex are less deeply weathered than the rocks of the adjacent Basement Complex. These attributes make it relatively easy to identify the Buji Younger Granite Complex both on the aeromagnetic map and the Landsat imagery. It forms a prominent topographic feature. The deep fractures control part of the drainage system of the area.

Acknowledgement

The authors wish to acknowledge the assistance of the Director and staff of National Centre for Remote Sensing Jos, who provided the landsat Imagery and allowed us access to some of the software and hardware used in this work. We are very grateful.

References

Buchanan, M. S., Macleod, W. N., Turner, D. C., Berridge, N. G., Black, K., 1971. The geology of the Jos plateau. Bull. Geol. Surv. of Nigeria, Vol. 2, No. 32, 168.

Falconer, J. D., 1911. The Geology and Geography of Northern Nigeria. Macmillian, London, 295.

Jacobson, R. R. E., MacLeod, W. N., Black, R., 1958. Ring Complexes in the Younger Granite Province of Northern Nigeria. Memoirs Geol. Soci., London, No. 1, 72 .

MacLeod, W. N., Turner, D. C., Wright, E. P., 1971. The Geology of the Jos Plateau. Bul Geol. Surv. of Nigeria, No. 32, Vol.1, 118.

Meer, F., Van der., 1997. Remote Sensing and GIS Techniques Applied to Geological Survey. In Integrated Land and Water Information System (ILWIS) 2.1 Application Guide, International Institute for Aerospace Survey and Earth Sciences, Publ., Enschede, 165-179.

Yakubu, H. M., 2005. Application of Geophysical Data and GIS in the Structural and Geological Mapping of the Buji Complex Area, Jos, Nigeria. Unpublished M. Sc. Thesis, University of Jos, Jos, Nigeria, 172.

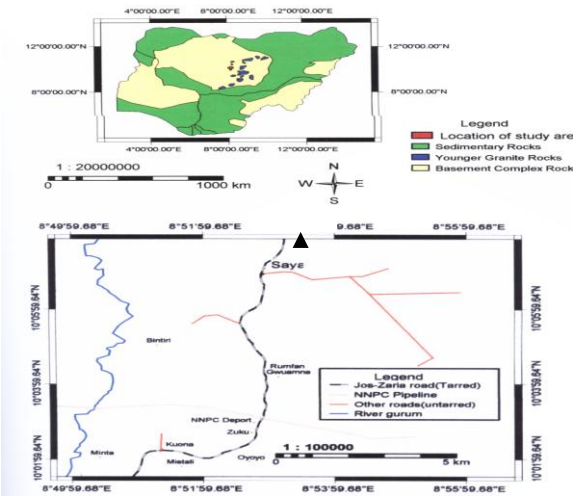

Fig. 1. Location map of Buji younger granite complex area.

To Jos (15km)

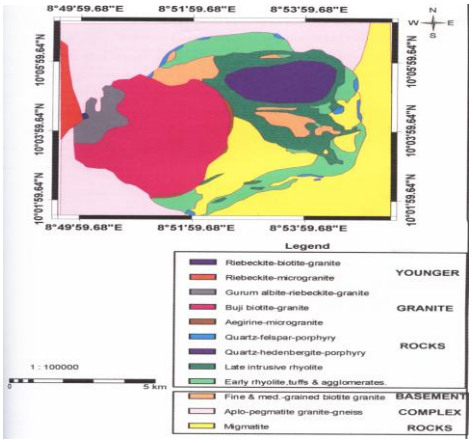

Fig. 2. Geological map of Buji area (After Buchanan et al., 1971).

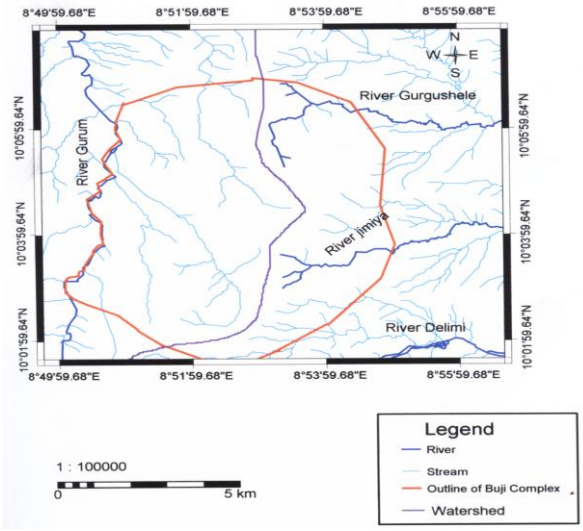

Fig. 3. Drainage system of Buji complex area.

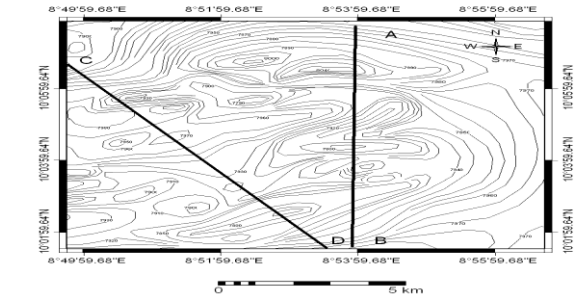

Fig. 4. Total intensity magnetic field map of Buji complex area.
Note lines of profile (AB, CD) across it.

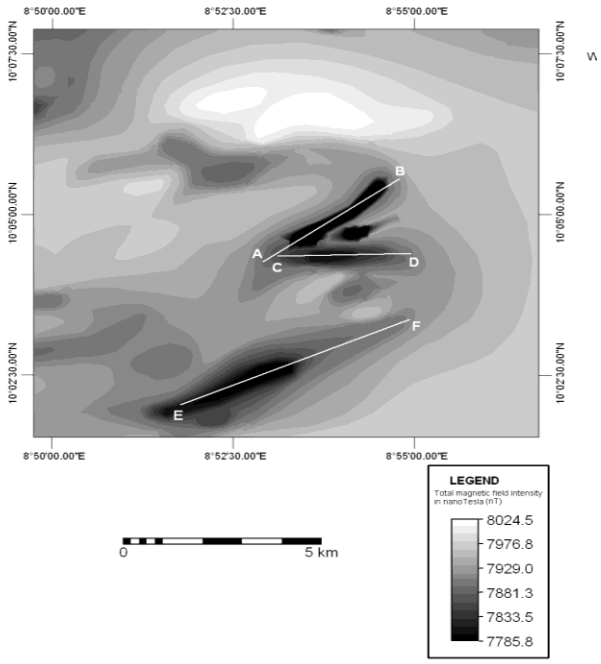

Fig. 5. Digital elevation model (DEM) showing magnetic lineaments: AB, CD and EF.

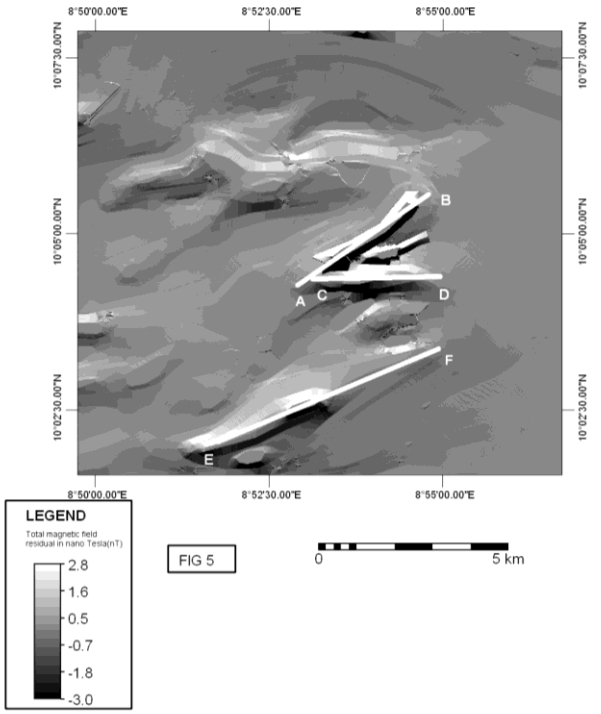

Figs. 6 and 7. Gradient filtered maps in the X (east) and Y(north) directions; Dfdx and Dfdy maps.

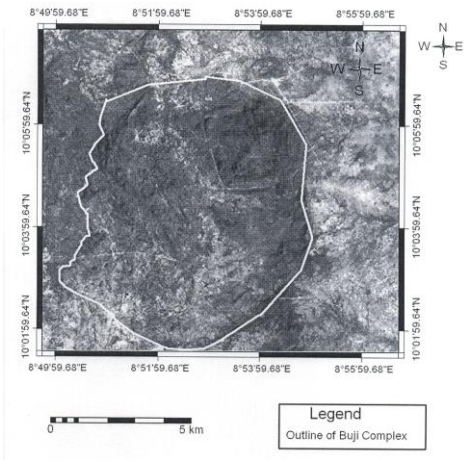

Fig. 8. Landsat imagery of Buji complex area.

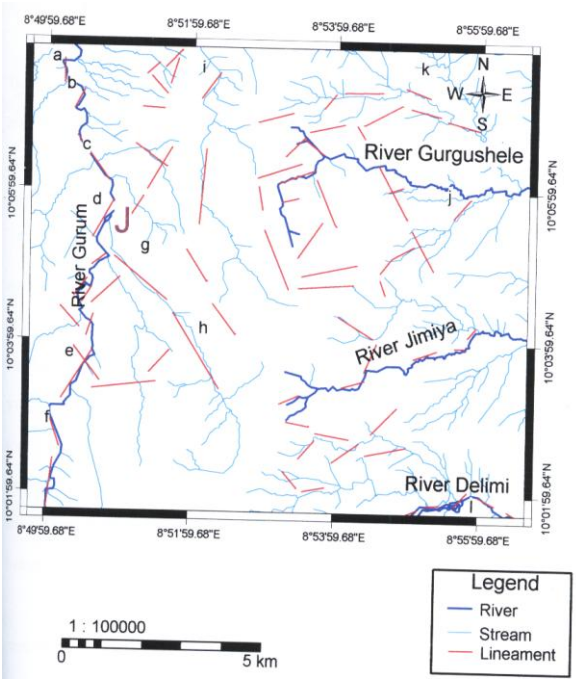

Fig.9. Lineaments draped on the drainage system of the Buji complex area.

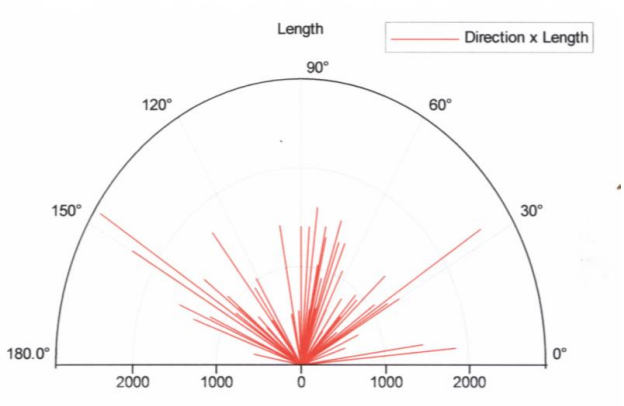

Fig. 10. Rose plot of the lineaments in Buji complex area.

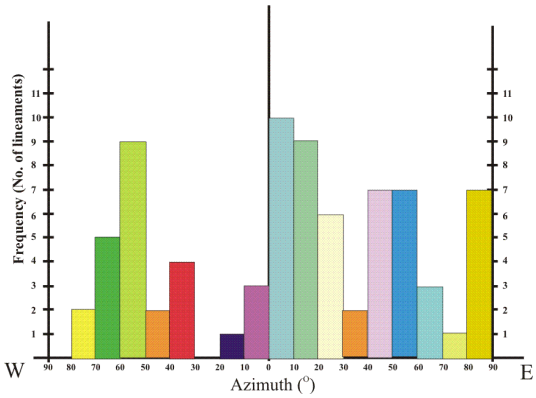

Fig. 11. Histogram of the lineaments in Buji complex area.

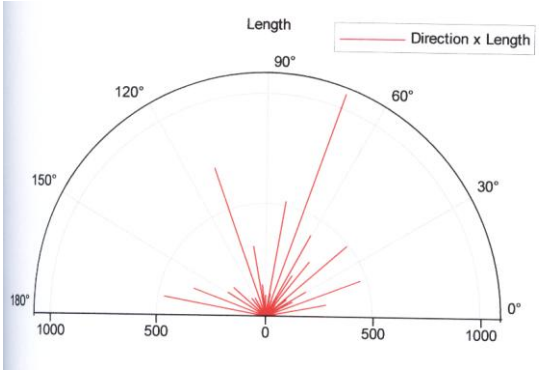

Fig. 12. Rose plot of the field fractures in Buji complex area.

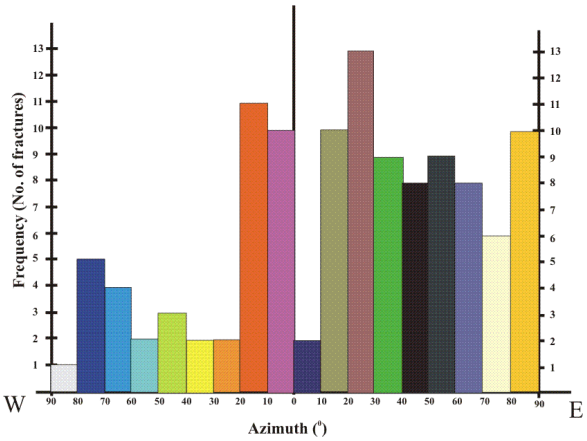

Fig. 13. Histogram of the field fractures in Buji complex area.